

PAPER • OPEN ACCESS

Self- and N₂- broadening of CO in the low-pressure regime

To cite this article: Y. Tan *et al* 2023 *J. Phys.: Conf. Ser.* **2439** 012007

View the [article online](#) for updates and enhancements.

You may also like

- [Rotation of Bloch sphere induced by Lamb shift in open two-level systems](#)
Guo-You Wang, , Ning Tang et al.
- [Numerical and experimental study of acoustic wave propagation in glass plate/water/128YX-LiNbO₃ structure](#)
Yota Terakawa and Jun Kondoh
- [Ultrasound bladder vibrometry method for measuring viscoelasticity of the bladder wall](#)
Ivan Z Nenadic, Bo Qiang, Matthew W Urban et al.

Self- and N₂- broadening of CO in the low-pressure regime

Y. Tan¹, T.-P. Hua¹, J.-D. Tang¹, J. Wang¹, A.-W. Liu¹, Y. R. Sun², C.-F. Cheng¹, S.-M. Hu¹

¹Department of Chemical Physics, University of Science and Technology of China, Hefei, 230026 China

²Institute of Advanced Science Facilities, Shenzhen 518107, China

E-mail: tanyan@ustc.edu.cn

Abstract. Sub-Doppler saturated absorption spectroscopy of rovibrational transitions of carbon monoxide broadened by nitrogen was recorded at low pressures (1-24 Pa) near 1.56 μm with comb-locked cavity ring-down saturation spectroscopy. We found a nonlinear pressure dependence of the Lamb-dip width of the CO transition induced by elastic scattering. Analysis of the results allows us to characterize parameters of elastic- and nonelastic- scattering under collisions. The elastic scattering angle for nitrogen-induced collisions (CO-N₂) was determined to be larger than 0.6×10^{-3} rad. The line broadening of the Lamb dip in the region of low pressures exceeds the broadening at high pressures by a factor of 4 and 5 for the self- and N₂-broadening CO R(9) transition. Moreover, much smaller line shifts for both self- and N₂-broaden Lamb dips were observed, which was also attributed to the decrease in the number of scattered molecules in the interaction and the increasing attracting forces.

1. Introduction

Lots of physical and chemical properties of a distant object could be obtained by interpreting its spectra. High-accuracy molecular absorption cross-section data are essential in astronomy, atmospheric science, and remote sensing [1]. Simulation of molecular absorption cross-sections requires line positions, intensities, and line shapes, regardless of spectral resolution. Compared to line position and intensity, line shape is more sophisticated to model since it has a complicated dependence on the environment of the molecules [2]. The well-known HITRAN database [3, 4] gives line-by-line spectroscopic parameters for high-resolution molecular absorption and radiance calculations. The database provides self- and air-broadening parameters for most atmospheric molecules, and foreign broadeners such as H₂, He, CO₂, and H₂O were included in recent years [5, 6, 7]. Limited by the experimental accuracy and sensitivity, most of the relevant data were derived from measurements of Doppler-broadened spectra at relatively high pressures ($10^2 - 10^5$ Pa). Line parameters, such as the Doppler width and collisional width, were obtained by fitting the spectra based on the particular lineshape model.

Saturated absorption spectroscopy allows to derive Doppler-free absorption profiles of molecules at low pressures. Early studies of nonlinear narrow transitions were mostly carried out with gas lasers in a saturated absorption cell inside the cavity. For instance, a CH₄ cell with a He-Ne laser around 3.39 μm [8, 9], and the CO₂ absorption with a CO₂ laser at 9.6 and 10.6 μm [10, 11], SF₆ and/or OsO₄ absorption with a CO₂ laser at 10.6 μm [12, 13]. One limitation of these measurements besides the stability of the laser frequency is the interference between the strong field and the nonlinear absorption since the gas cell is inside the laser cavity. Cavity-enhanced spectroscopy provides not only high sensitivity to measure weak absorption lines, but also high laser power to saturate the transition. Comb-referenced cavity-enhanced Lamb-dip measurements of C₂H₂ transitions near 1.5 μm were measured



through 1-f wavelength modulated absorption spectroscopy with a frequency accuracy of 10 kHz by Twagirayezu *et al.* [14]. The combination of saturated spectroscopy and cavity ring-down spectroscopy (CRDS) provides a new way to measure the nonlinear absorption, which was reported by Giusfredi *et al.* [15]. Recently, comb-locked saturated absorption cavity ring-down spectroscopy [16, 17] was applied to determine the 30013-00001 band of CO₂ and line frequencies with an accuracy of a few kHz were reported [18]. Frequencies of lines in the 30012-00001 band of CO₂ were determined with sub-kHz precision [19]. Coincidentally, line broadening coefficients of the lines obtained in these sub-Doppler spectroscopy measurements were found to be several times larger than those derived from Doppler-limited spectra.

Here we report a systematic study of the Doppler-free spectroscopy of the R(9) transition in the (3-0) band for samples of pure CO and CO mixed with N₂. Line broadening effects in the Lamb dips at the low-pressure regime are discussed in the following sections.

2. Experimental

Configuration of the experimental setup is shown in Fig. 1. It is similar to our previously developed comb-locked cavity ring-down saturation spectrometer [16, 17] and will be only briefly described here. A tunable external-cavity diode laser (ECDL, Toptica DL Pro-1550) was used as the probe laser, locked with a ring-down (RD) cavity through the Pound-Drever-Hall (PDH) method. A pair of high-reflective mirrors ($R = 99.997\%$ at 1.5-1.7 μm , Layertec GmbH Inc.) composed the RD cavity with a distance of 44.6 cm, leading to a free-spectral range of 336 MHz, a finesse of 1.36×10^5 , and a mode width of 2.2 kHz. A piezo actuator (PZT) stabilized the cavity length through a phase-lock circuit based on the beat signal between the probe laser and an optical frequency comb. The p -polarization probe laser beam, frequency shifted by an acousto-optical modulator (AOM) and a fiber electro-optical modulator (EOM), was coupled into the RD cavity from the other side of the cavity, thereafter produced the ring-down signal. The AOM also served as a beam chopper to trigger the ring-down event.

The recorded ring-down curve was fitted to an exponential decay function to derive the decay time τ . And the sample absorption coefficient would be determined as $\alpha = (c\tau)^{-1} - (c\tau_0)^{-1}$, where c is the speed of light, and τ_0 is the decay time of the empty cavity. The minimum detectable absorption coefficient α_{min} in this experiment was about $3 \times 10^{-11} \text{ cm}^{-1}$. Note that due to the saturation effect, the observed decay signal deviates from the single-exponential decay function. In principle, the saturation effect could be considered in the fitting procedure, as shown by Giusfredi *et al.* [15]. We also observed the line profile changing with the incident laser power. For simplicity, we still use the single-exponential decay function to fit recorded decay curves. Since the saturation parameter S is relatively small in our measurements (see text below), we found that the systematic deviation of the line width obtained in this way is within 5-10%, which will not affect the results obtained in this work.

The beat signal between the probe laser and an optical frequency comb was recorded, and it was used to lock the cavity length referring to a preset frequency f_B . The spectral scan was accomplished by tuning the reference frequency f_B ,

$$\nu = f_0 + n f_r + f_A + f_E + f_B, \quad (1)$$

where f_A and f_E are radio frequencies driving the AOM and EOM, and f_0 and f_r are the carrier offset frequency and repetition frequency of the optical comb, respectively. All radio frequencies were referenced to a GPS-disciplined rubidium clock (SRS FS725). When the phase-lock servo is turned on, the short-term fluctuation of the beat frequency f_B was less than 1 kHz ($\Delta\nu/\nu \sim 5 \times 10^{-12}$), indicating that the thermal drift of the ring-down cavity and the vibration noise had been compensated.

3. Results and discussions

3.1. Lamb-dip spectra and lineshape fitting

The rovibrational transition of ¹²C¹⁶O R(9) in the 3-0 overtone band was investigated in this experiment with self-broadening in the range of 0.04-2.0 Pa and nitrogen broadening in the range of 1-24 Pa at

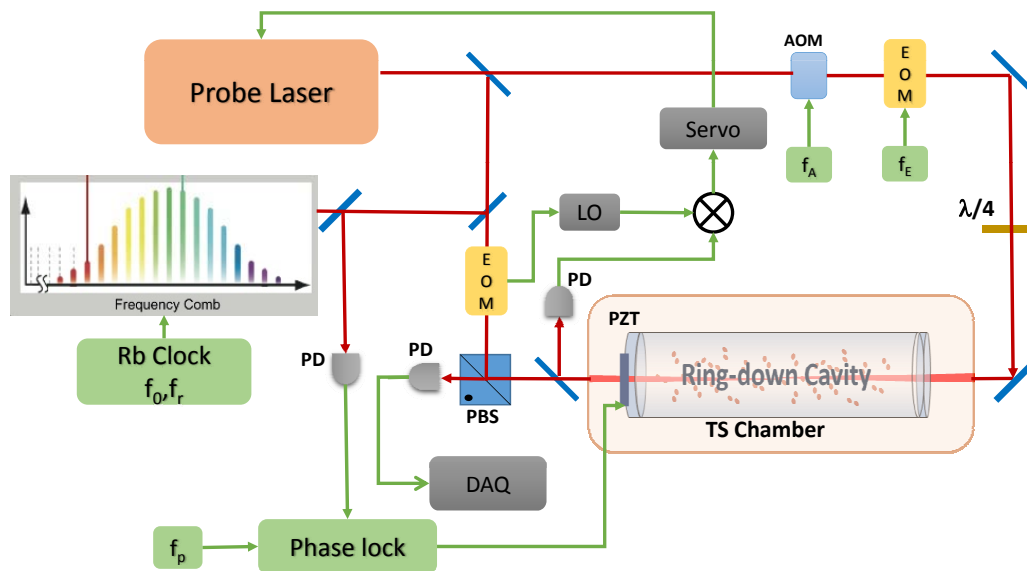


Figure 1. Scheme of the experimental setup. The red and green lines indicate the probe laser and control signal, respectively. Abbreviations: Probe Laser: ECDL, Toptica DL Pro-1550; DAQ: data acquisition system; PD: photodiode detector; LO: local oscillator; EOM: electro-optical modulator; PZT: piezo actuator; AOM: acousto-optical modulator; PBS: polarizing beam splitter; TS-chamber: temperature-stabilized chamber.

room temperature of about 294.5 K. Natural carbon monoxide and nitrogen sample gases were used in the experiment. Pressures of the carbon monoxide sample gas were calibrated from the absorption integral areas recorded from the Doppler broadened spectra with a fractional accuracy of about 1 %. Pressures of the nitrogen buffer gas were measured by a pressure gauge with an accuracy better than 0.5 %. Note that partial pressures of CO in all nitrogen broadening measurements were fixed around 1 Pa. We measured the self-broadened CO Lamb dips before we prepared gas mixtures with different nitrogen concentrations. The recorded saturated absorption spectra of pure CO were shown in Fig. 2, and nitrogen-broadened spectra were presented in Fig. 3.

We have applied both Voigt and Lorentz line profiles to fit the recorded saturated spectra. As shown in the lower panel of Fig. 2, relative fitting residuals for both line profiles are within the experimental uncertainty and identical to each other in the low-pressure region. Therefore, the line shape of the measured saturated absorption was described by a simple Lorentz profile. However, the Lamb dip is located on top of the Doppler-broadened absorption spectrum which has a Voigt line profile. We used the line shape of the Lamb dip taking into account the homogeneous power broadening [20] and the background of a Doppler broadened spectrum:

$$\alpha_S(\nu) = \alpha_e + \alpha_0(\nu) \frac{\Gamma}{B * \sqrt{1 - \left[\frac{2(\nu - \nu_0)}{A+B} \right]^2}}$$

$$A = \sqrt{(\nu - \nu_0)^2 + \Gamma^2}$$

$$B = \sqrt{(\nu - \nu_0)^2 + \Gamma^2(1 + 2S)}, \quad (2)$$

Where $\alpha_S(\nu)$ is the measured absorption coefficient, α_e is the baseline of the empty cavity, $\alpha_0(\nu)$

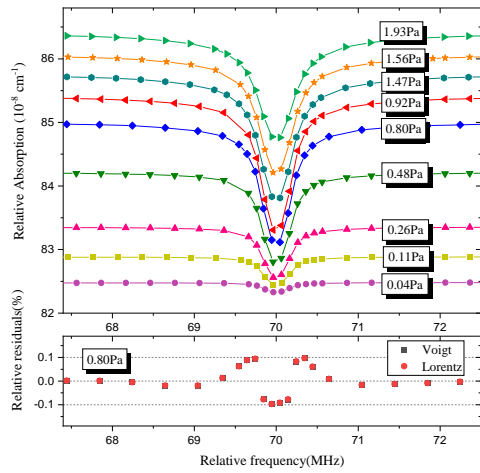


Figure 2. Lamb-dip spectra of the R(9) transition of pure CO with pressures of 0.04-2.0 Pa. The lower panel shows the relative fitting residuals from both Voigt and Lorentz line profiles for the spectra recorded at 0.8 Pa.

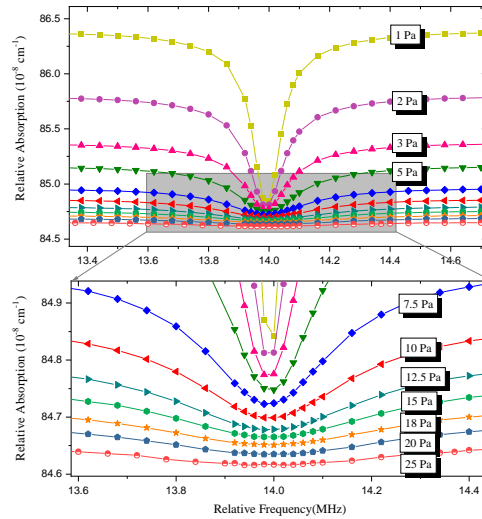


Figure 3. The Lamb-dips of the R(9) transition of CO in collision with the perturber N_2 were measured by cavity ring-down spectroscopy in the nitrogen pressure range of 1-25 Pa. The partial pressure of CO in all cases was around 1 Pa.

is the Doppler-broadened absorption coefficient described by a Voigt profile, Γ corresponds to the homogeneous width (half width at half maximum, HWHM) of the Lamb dip, and S is the saturation parameter. The Doppler-broadened spectra $\alpha_0(\nu)$ are described with line intensity from HITRAN2016 [3] and line broadening parameters from Predoi-Cross et al. [21] and they are sharing the same line center with the measured Lamb dips. The fitted results of the line widths, as well as the power saturation parameter S for both self- and N_2 -broadening of CO R(9), are listed in Table 1 and Table 2.

As been characterized in previous studies of Doppler-free spectroscopy [8, 11, 14, 22], the elastic scattering of particles dominates the behavior of the line width. Therefore, we focus on the direct contribution of the elastic collision process to the collisional scattering of molecules at low pressures of around 1 mTorr. Self-broadened CO Lamb dips were recorded with an input laser power of 0.8 mW and a pressure in the range of 0.04-1.9 Pa as plotted in Fig. 2, and Lorentzian profiles with Voigt absorption background were applied to fit the spectra. The line widths of the self-broadened CO R(9) Lamb-dips as well as corresponding saturation parameter S were given in Table 1. Together with the results from N_2 -broadened CO R(9) Lamb-dips at different nitrogen concentrations seen in Fig. 3 and Table 2, we determined the N_2 -broadened line width Γ_{N_2} for the CO R(9) transition deducting the self-broadened line width Γ_{self} from the line width of gas mixtures Γ_{mix} .

The results, as well as the saturation parameters of N_2 -broadened CO R(9) Lamb dips, were listed in Table 2. A nonlinear dependence of the collisional broadening width of Γ_{N_2} on the pressure of N_2 was observed as shown in Fig. 4 and the evolution of the Lamb-dip width from low to high pressures was discussed in the following section.

3.2. Collisional broadening of Lamb dips

There are various sources that result in broadening a transition in the gas phase, as listed in table 3. The Doppler effect results in hundreds of megahertz inhomogeneous broadening, which is absent in Lamb-

Table 1. Parameters of self-broadened Lamb dips of R(9) of CO.

P(CO) (Pa)	Γ (MHz)	S	v_0^* (kHz)
0.04	0.103(8)	1.244(202)	-1.6(27)
0.11	0.107(10)	1.233(247)	0.3(20)
0.26	0.135(16)	0.477(93)	-0.1(19)
0.49	0.154(5)	0.384(22)	0.5(32)
0.80	0.179(4)	0.252(7)	-0.4(17)
0.92	0.185(4)	0.237(7)	0.1(13)
1.47	0.223(4)	0.108(2)	-0.7(13)
1.56	0.229(6)	0.097(3)	-0.3(23)
1.93	0.257(4)	0.063(1)	-0.7(15)

* v_0 corresponds to the line center shift from 191 360 212 763.7 kHz.

Table 2. Line widths of N₂-broadened R(9) Lamb dips of CO under different N₂ pressures (CO pressure: 1 Pa).

P(N ₂) (Pa)	Γ_{total} (MHz)	S_{total}	Γ_{self}^* (MHz)	S_{self}^*	$\Gamma_{N_2} = \Gamma_{total} - \Gamma_{self}$ (MHz)
1.0	0.264(2)	0.136(3)	0.186(2)	0.245(8)	0.078(3)
1.9	0.353(4)	0.072(1)	0.192(3)	0.210(9)	0.161(5)
3.1	0.470(4)	0.043(1)	0.189(2)	0.218(6)	0.281(4)
4.9	0.638(6)	0.031(1)	0.184(2)	0.247(5)	0.454(6)
7.3	0.839(10)	0.018(1)	0.186(2)	0.224(5)	0.653(10)
9.7	1.007(14)	0.015(1)	0.167(2)	0.353(12)	0.840(14)
12.1	1.169(26)	0.011(1)	0.169(4)	0.355(21)	1.001(26)
14.6	1.341(35)	0.007(1)	0.185(2)	0.236(4)	1.157(35)
17.5	1.516(52)	0.006(1)	0.183(1)	0.257(5)	1.334(52)
19.4	1.625(74)	0.005(1)	0.191(2)	0.211(7)	1.433(74)
24.2	1.916(157)	0.002(1)	0.229(3)	0.098(3)	1.687(157)

* Γ_{self} , S_{self} represent HWHM and saturation parameter of the self-broadened Lamb dip with pure CO sample pressure of about 1 Pa except for $P(N_2) = 24.2$ Pa with $P(CO) = 1.6$ Pa.

dip measurements. Vibration-rotation energy levels of molecules usually have long lifetimes, leading to very narrow natural line widths (typically below 1 kHz). In the low-pressure range, the free path length is larger than the laser beam diameter, which makes the transit-time broadening dominate in the observed Lamb-dip spectrum. The transit-time broadening given by Demetröder [23], $\sqrt{2 \ln 2} v_p / 2\pi w_0$, results in $\gamma_t = 156.8$ kHz, while the expression for transit-time broadening from Bordé and Hall [24] gives $\gamma_t = 104.6$ kHz with $\gamma_t = v_p / 8w_0$. In addition, the effect of molecules colliding with the walls of the sample cell also induces extra line broadening. As shown in Table 3, the estimated value for the wall-collisional broadening width is about 2.1 kHz. The intercept obtained from fitting the self-broadened CO Lamb dips is about 113.1 kHz seen in Fig. 4, which represents the total pressure-independent line width from transit-time and wall-collisional broadening. In general, they agree with the estimated pressure-independent line width of about 106.7 kHz if we assume the transit-time broadening approaching from Bordé and Hall. The power saturation parameters could be fitted from the line shape of the Lamb dip Eq.2. As shown in Table 2, the collisional line width contributed from the perturber molecule N₂ was derived from the difference between dip widths of the CO-N₂ mixture and pure CO,

Table 3. Inhomogeneous and homogeneous line broadening for the Lamb-dip spectrum of the R(9) (3-0) line of CO.

Source	Line width (HWHM)	this work
Doppler	$\sqrt{\frac{2\ln 2 k_B T}{mc^2}} v_0$, ¹	Doppler free
Natural	$(2\pi\tau)^{-1}$	1.2 mHz
Collisional	$(\pi\tau_{coll})^{-1}$, ²	nonlinear: 90-20 kHz/Pa
Wall-Collisions	$\frac{u}{2\pi L}$, ³	2.1 kHz
Transit-time	$\frac{\sqrt{2\ln 2}}{2\pi} \frac{v_p}{w_0}$ or $\frac{v_p}{8w_0}$, ⁴	156.8 kHz/104.6 kHz
Power Saturation	$\gamma_s = \gamma\sqrt{1+S}$, ⁵	$0.001 \leq S < 1.2$

¹ v_0 : line center of the transition;

² τ_{coll} : mean time between collisions;

³ $u = \sqrt{\frac{8k_B T}{\pi M}}$, average thermal velocity of colliding particles, $L = 35\text{mm}$ diameter of sample cell;

⁴ $v_p = \sqrt{\frac{2k_B T}{m}}$, the most probable velocity, $w_0 \approx 0.5\text{mm}$ beam diameter;

⁵ S is the saturation parameter.

after taking into account the correction of saturation parameter in the Lamb dip line profile. Widths of self- and N_2 -broadened CO R(9) lines at different pressures were plotted in Fig. 4. We can see an almost linear dependence of the self-broadening line width against pressure on the upper panel, while the N_2 -broadened line width shows a nonlinear dependence on the N_2 pressure.

The physical picture of nonlinear optical resonance had been presented in previous studies [11, 22]. It has been demonstrated that the elastic scattering of particles causes the nonlinear dependence of the resonance width in the low-pressure regime. In elastic collisions, the kinetic energy of molecules is reserved which does not cause phase disturbances in the oscillator. While for inelastic collisions, the kinetic energy is transferred to rotational energy in the oscillator, which gives rise to phase perturbing and results in normal line broadening in a Doppler contour.

We can use the scattering angle of elastic collisions θ to explain the process for a small dip width with $\Gamma < \theta ku$, where Γ is the dip width, k is the wave vector, and u corresponds to the average speed of the colliding particle. The line broadening is a result of both elastic and inelastic processes. The contribution of elastic scattering broadening decreases with the density of particles, which explains the nonlinear dependence of resonance width on pressure. When the dip width increases with the pressure and reaches the case of $\Gamma > \theta ku$, the elastic collision-induced broadening becomes less significant.

According to early theoretical studies of the collision-induced broadening [11], the pressure-dependent Lamb-dip width could be determined by the total scattering cross-section:

$$\Gamma = \Gamma_0 + nu(\sigma_e + \sigma_n), \quad (3)$$

where Γ_0 is the line width independent of collisions, mainly from the transit-time broadening, n corresponds to the number density of colliding particles, σ_e is the elastic scattering cross-section, and σ_n is the inelastic scattering cross-section. The above Eq. (3) changes in the high-pressure regime where $\Gamma > \theta ku$, and the inelastic process becomes dominant which eventually turns to normal pressure-induced line broadening in the Doppler contour, while Γ_e induced by the elastic process turns to be a constant value:

$$\Gamma = \Gamma_0 + \Gamma_e + nu\sigma_n, \quad (4)$$

Among the line broadening mechanisms given in Table 3, only the collision-induced broadening is proportional to the number density of colliding particles, and other effects are independent of the pressure. Therefore, we could have the dip width for CO perturbed by N_2 determined through:

$$\Gamma = \Gamma_0 + \Gamma_{self} + \Gamma_{\text{N}_2} \quad (5)$$

$$\Gamma_{N_2} = nu(\sigma_e + \sigma_n), \quad (6)$$

Note that the self-broadened CO dipo and N₂-induced broadening were measured separately in this work. Comparing the equations above, we can find that the pressure-dependent broadening coefficient in the low-pressure regime would be larger than that at high pressures, and there is a ratio of $(\sigma_e + \sigma_n)/\sigma_n$ between these two values.

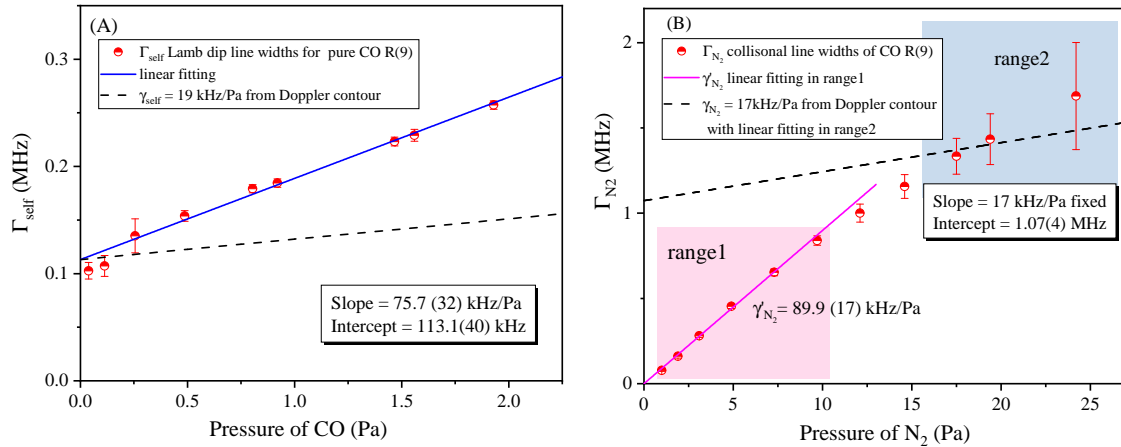


Figure 4. Pressure dependence of the Lamb-dip width of the CO R(9) transition in pure CO and CO-N₂ mixture. (a) Half width at half maximum of the line of pure CO against the pressure. The blue solid line shows a linear fit of the data, and the black dash line corresponds to the self-broadening coefficient obtained from Doppler-broadened spectroscopy at high pressures by Predoi *et al.* [21] (b) Nonlinear dependence of the N₂-induced CO line width (red dots) on the pressure of N₂. The magenta solid line shows the linear fit of the data in low pressures (< 10 Pa), and the black dash line shows the linear fit of the data in the range of 17-24 Pa, where the slope was fixed to be 17 kHz/Pa as the N₂-broadening coefficient obtained from Doppler-broadened spectroscopy at high pressures by Predoi *et al.* [21]

The nonlinear dependence of the collisional line width at low pressures provides us with a way to measure the scattering potential at long distances. The widths of CO self-broadened R(9) transition in the low-pressure range show almost linear dependence on pressure, the slope of data at low pressures obtained in this work is found to be 75.7 kHz/Pa for Γ_{self} seen in Fig. 4(A). And the self-broadening coefficient obtained from Doppler-broadened measurements at relatively high pressures is 19 kHz/Pa, as given by Predoi *et al.* [21] Therefore, a factor of 4 is determined for $(\sigma_e + \sigma_n)/\sigma_n$ in the self-broadened CO R(9) Lamb dipo. The intercept from the linear fit of self-broadened line widths is 113.1 kHz. According to Eq. 3, it is attributed to the pressure-independent line width Γ_0 . The value is just slightly larger than the sum of the transit-time broadening and wall-collisional broadening given in Table 3. The discrepancy may come from the uncertainty of the estimated beam diameter in the ring-down cavity. Fig. 4(B) shows the N₂ collision-induced line widths at different pressures, and we can see an apparent nonlinear dependence. The slope of the data at low pressures (as the red solid line in Fig. 4(B) for pressures < 10 Pa) is about 5 times larger than the value of 17 kHz/Pa obtained from Doppler-broadened measurements at high pressures [21]. The black dash line in Fig. 4(B) shows the linear fit in relatively high pressures (17-24 Pa) with the slope fixed as 17 kHz/Pa.

In accordance with Eq. 6, the total collisional scattering cross-section from nitrogen is:

$$\sigma_e + \sigma_n = \frac{1}{u} \cdot \frac{d\Gamma_{N_2}}{dn}, \quad (7)$$

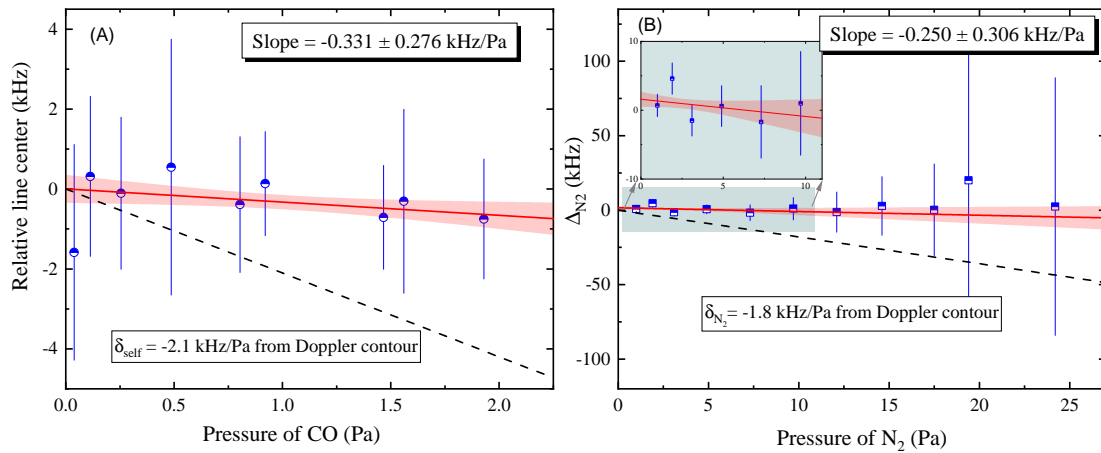


Figure 5. (a) Relative center frequencies of pure CO Lamb dips at different pressures of CO, the red line shows the linear fit of pressure-induced line shift; (b) The N_2 -induced line shift of the CO R(9) transition at different N_2 pressures with a fixed CO pressure of 1 Pa, and the red line shows the linear fit of the line shift. The plot in the blue shadow shows the zoomed-in plot at low pressures (< 10 Pa). Black dash lines correspond to the self-broadening and N_2 -broadening line-shift coefficients given by Predoi *et al.*[21]

We could determine the total scattering cross-sections in low and high number densities, which yield 78 \AA^2 and 15 \AA^2 , respectively. And the value of θ can estimate to be larger than 0.6×10^{-3} rad.

3.3. Pressure-dependent shift of the Lamb dip

In the previous sections, we discussed the nonlinear dependence of the Lamb-dip line widths on the pressure due to the elastic scattering of colliding molecules. A similar nonlinear character of the pressure-dependent line shift would also be expected. The effect was observed in the early study of a nonlinear methane absorber around $3.39 \mu\text{m}$ using a He-Ne laser [8]. They reported an anomalous sharp decrease in the shift of the Lamb dip of methane to less than 10 Hz/mTorr , which was attributed to the decrease in the number of scattered molecules in the interaction and the increasing attraction forces. A qualitative physical picture of this anomalous decrease in the shift could be described as follows. In the case where $\Gamma < \theta ku$, the colliding particle will not interact with the field after collisions. Consequently, the nature of resonance broadening will not be affected by the phase mismatching during collisions. With $\Gamma > \theta ku$, particles continue to interact with the field after the collision, which leads to phase mismatching and results in a resonance shift. The collisional shift in the low-pressure regime can decrease by more than one order of magnitude compared to that observed in Doppler-limited measurements. That is essential for gas laser frequency stabilization [8, 9, 20].

Shifts of the Lamb-dip centers were determined through the beating frequency referenced to the frequency comb in this work. Fig. 5(A) plotted relative shifts of the Lamb dips for pure CO, as well as gas mixtures of CO and N_2 . Line centers of pure CO samples were determined with uncertainties of a few kHz, and a linear fit of the experimental results indicates a slope much smaller than that yielded by Doppler-broadened studies. Spectra of CO- N_2 mixtures were treated similarly, and the results are shown in Fig. 5(B). The observed small shifts in low-pressure regime agree with previous studies [8] and coincide with the case where $\Gamma < \theta ku$.

4. Conclusions

Comb-locked cavity ring-down saturation spectroscopy was used to record the collisional broadening of CO transitions in the low-pressure regime. We were able to reveal how selective scattering affects the

resonance shapes where a nonlinear pressure dependence of the line width was observed. The change of the line width on pressure from the low-pressure regime to the normal Doppler contour allows us to characterize parameters of elastic- and nonelastic- scattering in collisions. In the absence of velocity changes in collisions, the line shape could be described by a Lorentzian function with a line width proportional to the density of perturbing particles. When the pressure is low enough ($\Gamma < \theta ku$), velocity-changing collisions break the equilibrium velocity distribution and introduce a frequency modulation. As a result, we would observe a nonlinear pressure dependence of the width and center of a rovibrational transition.

Acknowledgments

This work was jointly supported by the National Natural Science Foundation of China (41905018, 21903080, 21688102), and by the Chinese Academy of Sciences (XDB21020100, XDC07010000).

References

- [1] Miller C E, Brown L R, Toth R A, Benner D C and Devi V M 2005 *Comptes Rendus Physique* **6** 876–887 ISSN 16310705 URL <https://linkinghub.elsevier.com/retrieve/pii/S1631070505001155>
- [2] Hartmann J M, Tran H, Armante R, Boulet C, Campargue A, Forget F, Gianfrani L, Gordon I, Guerlet S, Gustafsson M, Hodges J T, Kassı S, Lisak D, Thibault F and Toon G C 2018 *Journal of Quantitative Spectroscopy and Radiative Transfer* **213** 178–227 ISSN 00224073 URL <https://doi.org/10.1016/j.jqsrt.2018.03.016>
- [3] Gordon I E, Rothman L S, Hill C, Kochanov R V, Tan Y, Bernath P F, Birk M, Boudon V, Campargue A, Chance K V, Drouin B J, Flaud J M, Gamache R R, Hodges J T, Jacquemart D, Perevalov V I, Perrin A, Shine K P, Smith M A, Tennyson J, Toon G C, Tran H, Tyuterev V G, Barbe A, Császár A G, Devi V M, Furtenbacher T, Harrison J J, Hartmann J M, Jolly A, Johnson T J, Karman T, Kleiner I, Kyuberis A A, Loos J, Lyulin O M, Massie S T, Mikhailenko S N, Moazzen-Ahmadi N, Müller H S, Naumenko O V, Nikitin A V, Polyansky O L, Rey M, Rotger M, Sharpe S W, Sung K, Starikova E, Tashkun S A, Auwera J V, Wagner G, Wilzewski J, Wcisło P, Yu S and Zak E J 2017 *Journal of Quantitative Spectroscopy and Radiative Transfer* **203** 3–69 ISSN 00224073
- [4] Gordon I, Rothman L, Hargreaves R, Hashemi R, Karlovets E, Skinner F, Conway E, Hill C, Kochanov R, Tan Y, Wcisło P, Finenko A, Nelson K, Bernath P, Birk M, Boudon V, Campargue A, Chance K, Coustenis A, Drouin B, Flaud J, Gamache R, Hodges J, Jacquemart D, Mlawer E, Nikitin A, Perevalov V, Rotger M, Tennyson J, Toon G, Tran H, Tyuterev V, Adkins E, Baker A, Barbe A, Canè E, Császár A, Dudaryonok A, Egorov O, Fleisher A, Fleurbaey H, Foltynowicz A, Furtenbacher T, Harrison J, Hartmann J, Horneman V M, Huang X, Karman T, Karns J, Kassı S, Kleiner I, Kofman V, Kwabia-Tchana F, Lavrentieva N, Lee T, Long D, Lukashvskaya A, Lyulin O, Makhnev V, Matt W, Massie S, Melosso M, Mikhailenko S, Mondelain D, Müller H, Naumenko O, Perrin A, Polyansky O, Raddaoui E, Raston P, Reed Z, Rey M, Richard C, Tóbiás R, Sadiek I, Schwenke D, Starikova E, Sung K, Tamassia F, Tashkun S, Vander Auwera J, Vasilenko I, Viganin A, Villanueva G, Vispoel B, Wagner G, Yachmenev A and Yurchenko S 2022 *Journal of Quantitative Spectroscopy and Radiative Transfer* **277** 107949 ISSN 00224073 URL <https://linkinghub.elsevier.com/retrieve/pii/S0022407321004416>
- [5] Wilzewski J S, Gordon I E, Kochanov R V, Hill C and Rothman L S 2016 *Journal of Quantitative Spectroscopy and Radiative Transfer* **168** 193–206 ISSN 00224073
- [6] Tan Y, Kochanov R V, Rothman L S and Gordon I E 2019 *Journal of Geophysical Research: Atmospheres* **124** 11580–11594 ISSN 2169-897X URL <https://onlinelibrary.wiley.com/doi/10.1029/2019JD030929>
- [7] Tan Y, Skinner F M, Samuels S, Hargreaves R J, Hashemi R and Gordon I E 2022 *The Astrophysical Journal Supplement Series* **262** 40 ISSN 0067-0049
- [8] Bagaev S, Baklanov E and Chebotayev V 1972 *Soviet Journal of Experimental and Theoretical Physics Letters* **16** 344–348 ISSN 0021-3640
- [9] Bagayev S N, Vasilenko L S, Dmitriyev A K and Gol V G 1976 *Appl. Phys.* **235** 231–235
- [10] Meyer T W, Rhodes C K and Haus H A 1975 *Physical Review A* **12** 1993–2008 ISSN 0556-2791 URL <https://link.aps.org/doi/10.1103/PhysRevA.12.1993>
- [11] VASILENKO L, KOCHANOV V and CHEBOTAYEV V 1977 *OPTICS COMMUNICATIONS* **20** 1–3
- [12] During M and Saturation A 1971 *SOVIET Physics JETP* **32** 2–7
- [13] Chardonnet C, Guernet F, Charton G and Bordé C J 1994 *Applied Physics B Lasers and Optics* **59** 333–343 ISSN 09462171
- [14] Twagirayezu S, Hall G E and Sears T J 2018 *Journal of Chemical Physics* **149** 154308 ISSN 0021-9606 URL <http://aip.scitation.org/doi/10.1063/1.5047410>
- [15] Giusfredi G, Bartalini S, Borri S, Cancio P, Galli I, Mazzotti D and De Natale P 2010 *Physical Review Letters* **104** 110801 ISSN 0031-9007 URL <http://link.aps.org/doi/10.1103/PhysRevLett.104.110801>

- [16] Wang J, Sun Y R, Tao L G, Liu A W, Hua T P, Meng F and Hu S M 2017 Review of Scientific Instruments **88** ISSN 10897623
- [17] Wang J, Sun Y R, Tao L G, Liu A W and Hu S M 2017 Journal of Chemical Physics **147** 091103 URL <http://www.ncbi.nlm.nih.gov/pubmed/28886636>
- [18] Wu H, Hu C L, Wang J, Sun Y R, Tan Y, Liu A w and Hu S m 2020 Physical Chemistry Chemical Physics **22** 2841–2848 ISSN 1463-9076 URL <http://xlink.rsc.org/?DOI=C9CP05121J>
- [19] Tan Y, Xu Y R, Hua T P, Liu A W, Wang J, Sun Y R and Hu S M 2022 Journal of Chemical Physics **156** ISSN 10897690
- [20] Letokhov V S and Chebotayev V P 1977 Nonlinear Laser Spectroscopy (New York: Springer-Verlag) ISBN 3-540-08044-9
- [21] Predoi-Cross A, Hnatovsky C, Strong K, Drummond J R and Chris Benner D 2004 Journal of Molecular Structure **695-696** 269–286 ISSN 00222860
- [22] Chebotayev V P 1985 Physics Reports **119** 75–116 ISSN 03701573
- [23] Demtroder W 1981 Laser Spectroscopy: Basic Concepts and Instrumentation (Berlin: Springer-Verlag)
- [24] Bordé C J, Hall J L, Kunasz C V and Hummer D G 1976 Phys. Rev. A **14** 236–263 ISSN 0556-2791 URL <https://link.aps.org/doi/10.1103/PhysRevA.14.236>